DOI: https://doi.org/10.34123/jurnalasks.v17i2.850

Available online at https://jurnal.stis.ac.id/

Jurnal Aplikasi Statistika & Komputasi Statistik
Vol. 17 No. 2, December 2025
e- ISSN: 2615-1367, p-ISSN:2086-4132

Satellite Imagery for Classification Analysis of Abrasion Areas on Panaitan, Banten

Ghaffar Ismail[1*], Robert Kurniawan[2], Silvia Ni'matul Maula[3]

[1,2]Politeknik Statistika STIS, Jakarta, Indonesia, [3]School of Public Policy and Management, Tsinghua University, Beijing, China
**Corresponding Author: E-mail address: 222112071@stis.ac.id*

ARTICLE INFO

Article history:
Received 30 September, 2025
Revised 6 December, 2025
Accepted 23 December, 2025
Published 31 December, 2025

Keywords:
Abrasion; Classification; Machine learning; Panaitan; Satellite imagery

Abstract

Introduction/Main Objectives: Abrasion causes severe environmental degradation and socio- economic losses, Waton and Karang Gundul Islands have already subsided due to erosion, posing risks to Panaitan Island, a national park that also faces deforestation, infrastructure development, and vegetation loss which may intensify abrasion. **Background Problems:** Limited spatial data on coastal abrasion in Panaitan Island hampers effective monitoring and management, highlighting the need for spatially explicit analysis. **Novelty:** This study identified and classified abrasion-prone areas on Panaitan Island (a rarely exposed island) with rarely variables which have impactful indices such as MVI, TCI, and LSWI. **Research Methods:** Landsat 8 and Sentinel-2 imagery from 2018 and 2023 were analyzed to assess changes in vegetation, mangroves, surface temperature, and soil moisture. Random Forest, Support Vector Machine, and Logistic Regression were employed to classify abrasion-prone areas. **Finding/Results:** The analysis revealed signs of abrasion covering 2.04 km², with Random Forest achieving the highest accuracy (82.23%) and NDVI as the most influential variable; abrasion was mainly associated with declining forest and mangrove cover, soil moisture showed weak correlation, while moderate surface temperature had a positive effect. Preventive measures such as reforestation and mangrove rehabilitation are recommended to mitigate risks and ensure long-term environmental sustainability.

1. Introduction

Shorelines are threatened by coastal abrasion, which also damages infrastructure and communities, jeopardizes human safety, and degrades the environment [1]. Land erosion in Europe reached about 4,500 km² between 1975 and 2006, and by 2050, it is expected to reach 5,800 km² [2]. Over one-third of China's coastline has been eroded, and in certain places, shoreline retreat can approach 300 meters annually [3]. It is also anticipated that Indonesia, which has more than 17,000 islands and 80,000 km of coastline, will be badly impacted. With 115 islands expected to be at risk of submersion by 2100 and 28 islands reported to have sunk in 2011, abrasion poses a concern to Indonesia's small islands [4]. Banten Province is one of the several coastal regions in Indonesia where abrasion is now occurring.

Karang Gundul Island and Waton Island were lost to coastal abrasion in 2015, according to the Banten Province Government [5]. Panaitan Island and other nearby islands may also be under danger due to this circumstance. According to the Republic of Indonesia's Decree of the Minister of Forestry

No. SK.3658/Menhut-VII/KUH/2014, issued May 5, 2014, regarding the Designation of the Ujung Kulon National Park Forest Area, Panaitan Island is a protected forest area that is home to a variety of plants and animals and is a well-liked destination for ecotourism and surfing. But there are now serious risks: the number of unlawful operations in Ujung Kulon National Park has increased dramatically, from 216 in 2019 to 680 in 2023. Abrasion can be accelerated by a variety of activities, including logging, illegal road construction, and the removal of vegetation [6].

Because their root systems prevent soil and sand from eroding, green vegetation, especially mangroves, is crucial in reducing abrasion [7]. Paradoxically, despite having the largest mangrove environment, Pandeglang Regency also saw the highest mangrove loss from abrasion, with 130.73 hectares lost in 2023 [8]. Rising sea levels and temperatures brought on by climate change make abrasion much worse [1]. These circumstances give rise to worries over possible abrasion on Panaitan Island, which may eventually cause the island to sink. Monitoring signs of abrasion on Panaitan Island is further hampered by the absence of island-level statistics and information as opposed to district/city- level data.

This study examines and categorizes regions that are prone to abrasions while examining important contributing elements. A number of indices are used, such as the Normalized Difference Vegetation Index (NDVI) for vegetation density [9], the Modified Normalized Difference Water Index (MNDWI) for shoreline changes using an overlay approach [10, 11], the Mangrove Vegetation Index (MVI) for detecting mangrove distribution [12], the Land Surface Temperature (LST) for tracking changes in surface temperature related to climate change [13], and the Land Surface Water Index (LSWI) for soil moisture conditions [14]. For classification modeling, machine learning techniques like Random Forest, Support Vector Machine (SVM), and Logistic Regression are used [15].

Various techniques for abrasion analysis and satellite image classification have been widely applied in related studies. One study assessed the influence of vegetation density on shoreline change using NDVI and DSAS and found that its effect was relatively small, accounting for only about 6.5% [16]. Another study comparing machine learning algorithms such as Random Forest, SVM, and stacking reported that SVM achieved the best performance, with accuracy reaching 0.983 [17]. Abrasion modeling using overlay and SWIR-1 techniques indicated a potential abrasion area of 118.50 hectares over a ten-year period [11]. Shoreline change analysis has also been conducted using tidal variables and linear regression methods [18]. In addition, the application of a Decision Tree algorithm using MNDWI, NDVI, EVI2, and GRVI variables resulted in an accuracy of 82.25% in coastal abrasion studies [19]. An integrated approach combining statistical techniques (EPR, AOR, and LR), remote sensing, and GIS achieved an RMSE of ±10 m [20]. Furthermore, in multispectral image classification, Random Forest produced the highest accuracy (81.2%) compared to Decision Tree and Rule-Based approaches [21].

This study is unusual because it combines remote sensing technology with a special set of indices like MVI, LSWI, and TCI—that are rarely used in earlier abrasion classification models. Imagery for each variable in this study was obtained from Landsat 8 and Sentinel-2. However, the study is limited by the omission of other variables that could affect abrasion, such as wave height. Additionally, it thoroughly examines the interactions between variables. Additionally, research concentrating on the risk of abrasion on a small island have not yet been conducted on Panaitan Island. It is anticipated that this study will provide light on how to stop small islands from being lost to abrasion. This work intends to create a machine learning-based categorization model of abrasion sites by identifying probable abrasion risks on Panaitan Island, taking into account factors including vegetation density, soil conditions, surface temperature, and mangrove distribution. In order to classify abrasion-prone areas of Panaitan Island using optimal machine learning techniques (Support Vector Machine, Random Forest, and Logistic Regression) with satellite imagery, this study aims to identify key variables for classifying abrasion areas and estimating impacted zones, while providing remote-sensing-based insights to support abrasion monitoring and mitigation on Panaitan Island.

2. Material and Methods

2.1. Data Source

The data were obtained from Sentinel-2 and Landsat imagery (Landsat-5, Landsat-7, and Landsat-8) accessed through the Google Earth Engine (GEE) Data Catalog to analyze shoreline abrasion on Panaitan Island. Shoreline abrasion was defined as the dependent variable and classified into abrasion and non-abrasion categories based on coastline overlay analysis, while the independent variables consisted of changes in the Mangrove Vegetation Index (MVI), Normalized Difference Vegetation Index (NDVI), Land Surface Water Index (LSWI), and Temperature Condition Index (TCI) observed from January 1 to December 31 in 2018 and 2023. A five-year observation interval was selected because

it is sufficient to capture abrasion dynamics compared to shorter periods [11,16]. The imagery was processed using annual median pixel values, which were averaged to generate a 20 m × 20 m spatial grid in QGIS. This spatial resolution was chosen to preserve detailed spatial variation while effectively covering coastal areas and is consistent with previous studies employing grid sizes of 50 × 50 m [22] and 10 × 10 m [23] for vegetation and erosion analyses. The characteristics of the variables and data sources used in this study are summarized in Table 1.

Table 1. Data sources

No.	Variable	Description	Sources	References
1.	X1	Change in Mangrove Vegetation Index (ΔMVI) 2018 and 2023	Sentinel-2	[12, 24, 25]
2.	X2	Change in Normalized Difference Vegetation Index (ΔNDVI) 2018 and 2023	Sentinel-2	[26]
3.	X3	Change in Land Surface Water Index (ΔLSWI) 2018 and 2023	Sentinel-2	[14, 27]
4.	X4	Change in Temperature Condition Index (ΔTCI) 2018 and 2023	Landsat-8	[28]
5.	Y	Change in Abrasion (1) and Non-Abrasion (0) Area Categories 2018 and 2023	Landsat-5,7,8	[10]

2.2. Analysis Method

The analytical procedure began with the preparation of satellite image data, including extraction, scaling, and categorization, followed by class balancing using the Synthetic Minority Over-sampling Technique (SMOTE) to address the lower number of abrasion samples compared to non-abrasion samples. The dataset was then divided into training and testing subsets. Exploratory data analysis was conducted using descriptive statistics, while variable distributions and relationships were examined through boxplots and correlation analysis, complemented by multicollinearity testing using correlation matrices and the Variance Inflation Factor (VIF), where VIF values greater than 10 indicate multicollinearity [29]. This step supports attribute selection and improves the stability and performance of machine learning models [30]. Abrasion classification was subsequently performed using Random Forest (RF), Support Vector Machine (SVM), and Logistic Regression, with optimal model parameters determined through Bayesian optimization and five-fold cross-validation. Model performance was evaluated using accuracy, precision, recall, and F1-score, supported by confusion matrix validation, georeferencing, and spatial visualization of the classification results. In addition, Feature Importance Ranking (FIR) was applied to assess the contribution of each variable, with RF and SVM selected based on their documented superior performance in satellite image classification [17,21], while Logistic Regression was included due to the binary nature of the abrasion classification.

2.2.1. Random Forest

Random Forest is an ensemble machine learning technique including many decision trees utilized for categorization purposes [31]. The method employed for identifying optimal parameters is Grid Search. This study's Random Forest encompasses n_estimators from 1 to 100, max_depth from 1 to 10, min_samples_split from 2 to 10, and min_samples_leaf from 1 to 10. Furthermore, there exists a bootstrap parameter with options of True or False, along with max_features varying from 0.1 to 1.

2.2.2. Support Vector Machine

The Support Vector Machine (SVM) seeks to identify the optimal separating hyperplane for precise data classification. The objective is to reduce classification errors in both training and unseen test datasets [32]. This study's SVM parameters consist of C values of 0.1, 1, and 10; gamma values of 1, 0, 0.1, and 0.01; and kernel options of 'rbf' and 'linear'.

2.2.3. Logistic Regression

Logistic regression is frequently selected for binary response models. Its reliance on chances facilitates interpretation, rendering the outcomes comprehensible to the general populace. Conversely, the probit and complementary log-log models are exclusively applicable to prospective data due to their dependence on probability [33]. This study's Logistic Regression settings comprise C values of 0.01, 0.1, 1, and 10; max_iter values of 100, 200, and 300; solver options of 'lbfgs', 'liblinear', and 'saga'; and class_weight options of None and 'balanced'.

2.2.4. Model Evaluation

The optimal machine learning model was selected to achieve the most effective categorization results for abrasion-prone areas. This study employed four primary metrics to evaluate model performance: accuracy, precision, recall, and F1-score [34]. The equations for each assessment metric are as follows:

$$Accuracy = \frac{TP+TN}{TP+TN+FP+FN} \quad (1)$$

$$Presicion = \frac{TP}{TP+FP} \quad (2)$$

$$Recall = \frac{TP}{TP+FN} \quad (3)$$

$$F1-Score = 2\,x\,\frac{Precision\,x\,Recall}{Precision+Recall} \quad (4)$$

where TP (True Positive) denotes the number of abrasion-prone areas correctly classified as prone, TN (True Negative) represents the number of non–abrasion-prone areas correctly classified as non-prone, FP (False Positive) refers to the number of non–abrasion-prone areas incorrectly classified as prone, and FN (False Negative) indicates the number of abrasion-prone areas incorrectly classified as non-prone.

3. Results and Discussion

This chapter aims to identify and analyze each change in variables in this study, after which a classification of abrasion and non-abrasion areas is carried out so that all existing information can be elaborated and analyzed. This study was performed on Panaitan Island, Ujung Kulon National Park, utilizing satellite imagery with a resolution of 20m x 20m. The abrasion on Panaitan Island was examined by overlay analysis. A total of 11,545 data records were collected, comprising 4,867 records in the abrasion category (1) and 6,678 records in the non-abrasion category (0).

3.1. Exploration of variables for changes in environmental conditions

Prior to modeling the classification of abrasion and non-abrasion zones, researchers examined the environmental conditions in Panaitan, focusing on changes that transpired between 2018 and 2023 as indicators or variables for the model.

3.1.1. Coastline

Shoreline abrasion in this study was identified through an overlay analysis of coastline maps derived from satellite imagery in 2018 and 2023, enabling the detection of coastline retreat as an indicator of abrasion. Grid cells with a spatial resolution of 20 m × 20 m were classified as abrasion (1) when they intersected areas showing coastline retreat—depicted as red zones between the two observation years—and as non-abrasion (0) otherwise, as illustrated in Figure 1. The spatial distribution reveals that multiple sections of Panaitan Island exhibit clear signs of abrasion, with the most pronounced changes occurring along the eastern coastline. This pattern suggests that the eastern coast is more exposed to wave action and hydrodynamic forces, making it particularly vulnerable to shoreline retreat over time.

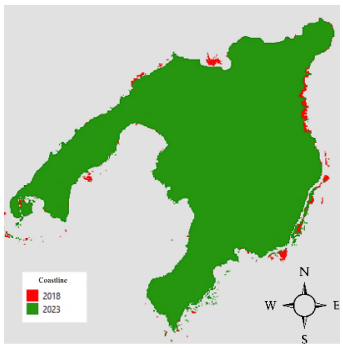

Figure 1. Map of indication of abrasion area of Panaitan Island

3.1.2. Mangrove Vegetation Index

The Mangrove Vegetation Index (MVI) assesses the health and spread of mangrove vegetation through the comparison of NIR, Green, and SWIR values. Mangroves serve as a significant signal closely associated with abrasion overall. The Mangrove Vegetation Index (MVI) assesses mangrove health, distribution, and density using Sentinel-2 data, calculated from the green, near-infrared (NIR), and shortwave infrared (SWIR) bands as: MVI = (NIR − Green) / (SWIR − Green) [12, 24, 25]. Figures 2(a) and 2(b) indicate that certain coastal regions of Panaitan Island possess mangrove vegetation. Nevertheless, in comparing the two years in th eir entirety, numerous regions exhibited a decline in mangrove vegetation. Moreover, an increased index value correlates with greater mangrove density. Mangroves function as wave breakers and enhance soil stability during significant wave events.

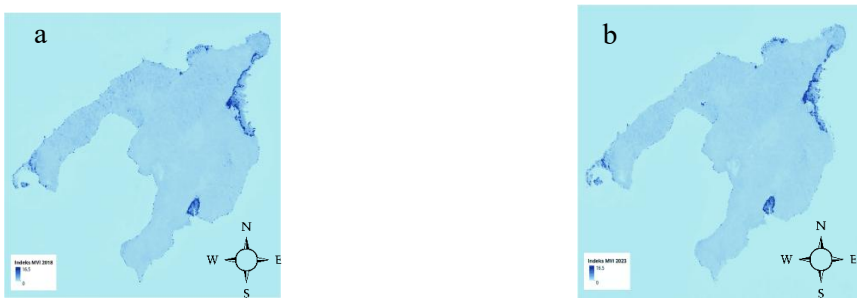

Figure 2. (a) MVI distribution map 2018 Panaitan; (b) MVI distribution map 2023 Panaitan

3.1.3. Normalized Difference Vegetation Index

Mangroves serve as a significant signal closely associated with abrasion overall. The Normalized Difference Vegetation Index (NDVI) monitors vegetation density with an index value range from -1 to +1. The Normalized Difference Vegetation Index (NDVI) assesses vegetation health using the red and near-infrared (NIR) bands and is calculated as (NIR − Red) / (NIR + Red) [35]. According to Figures 3(a) and 3(b), from 2018 to 2023, certain regions of the coast of Panaitan Island, specifically the southwest and east, exhibited a diminishing green hue, signifying a reduction in vegetation density. In contrast, the central portion of the forest retained its density and verdancy due to the absence of residential developments.

Figure 3. (a) NDVI distribution map 2018 Panaitan; (b) NDVI distribution map 2023 Panaitan

3.1.4. Land Surface Water Index

The Land Surface Water Index (LSWI) is used to measure soil moisture with an index range of -1 to +1. The Land Surface Water Index (LSWI) evaluates current soil moisture using the near-infrared (NIR) and shortwave infrared (SWIR) bands and is calculated as (NIR − SWIR) / (NIR + SWIR) [14]. Figures 4(a) and 4(b) demonstrate that negative vegetation index values signify aquatic regions, including beaches and the ocean. From 2018 to 2023, Panaitan Island's coastline witnessed a reduction in vegetation density, however the interior forest retained its density and verdancy due to the absence of settlements. In the figure, there is an indication that the 2018 image appears darker. This may be because throughout that year, the dry season was more dominant, resulting in lower LSWI values, which appear darker. Conversely, during years with a longer rainy season, LSWI values are generally higher and therefore appear brighter. The imagery in GEE has been processed using a cloud-mask filter to remove clouds as effectively as possible, and the images shown represent the best results obtained in this study for the LSWI imagery.

Figure 4. (a) LSWI distribution map 2018 Panaitan; (b) LSWI distribution map 2023 Panaitan

3.1.5. Temperature Condition Index

The Temperature Condition Index (TCI) assesses coastal thermal pressure. The TCI index spans from 0 to 100, indicating that a value closer to zero corresponds to a higher surface temperature pressure. The Temperature Condition Index (TCI) evaluates drought conditions using land surface temperature (LST) and is calculated as $((LST_{max} - LST_i) / (LST_{max} - LST_{min})) \times 100$ [13]. Figures 5(a) and 5(b) show a striking difference in the surface temperature index between sea and land in 2018 and 2023. Higher TCI values indicate cooler and more stable temperatures, with islands having higher values due to the presence of forests. Overall, 2018 had more areas with cooler temperatures than 2023, although the average coastal TCI showed the opposite. There are several limitations when using satellite imagery, one of which is the presence of clouds. However, in this study, a cloud-mask filter in GEE was applied and tested multiple times, and the images shown above represent the best results obtained for the TCI imagery.

Figure 5. (a) TCI distribution map 2018 Panaitan; (b) TCI distribution map 2023 Panaitan

3.1.6. Relationship Between Variables

All independent variables have a correlation of less than 0.8 with one another. Abrasion exhibits a negative correlation with alterations in NDVI (-0.49) and MVI (-0.24), suggesting that a decline in vegetation and mangrove density heightens the risk of abrasion. LSWI exhibits a correlation of 0.00,

signifying an absence of linear association with abrasion. TCI exhibits a positive correlation of 0.23, suggesting that regions with declining surface temperatures are more prone to abrasion; however, this value may be affected by external variables such as climate change or pandemics, as illustrated by the correlation coefficients in Figure 6.

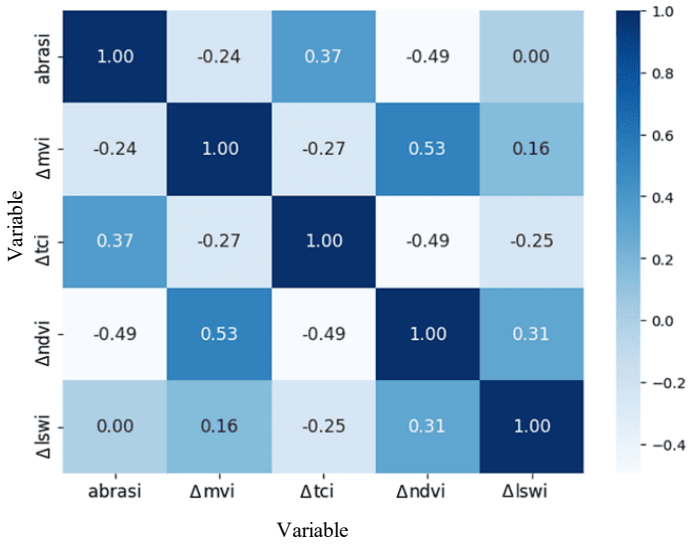

Figure 6. Heatmap of correlation coefficient between variables

3.1.7. Characteristics of Abrasion and Non-Abrasion Area Categories

The index delta is calculated by subtracting the 2018 index from the 2023 index; thus, a negative value indicates that the 2023 index is lower than the 2018 index, and vice versa. According to Table 2, the abrasion zone on Panaitan Island exhibits an average decline in NDVI and MVI, signifying a reduction in the density of green vegetation and mangroves that mitigate abrasion, this could be caused by illegal activities that occur in the Ujung Kulon area, one of which is Panaitan Island such as logging, land clearing, and resource extraction. The variation in LSWI is minimal between the abrasion and non-abrasion zones; however, the abrasion zone appears drier in 2023 owing to diminished water-retaining vegetation. The TCI in the abrasion zone is positive, signifying that the surface temperature in 2023 was lower than in 2018, potentially affected by external forces such as the pandemic that diminished human activity [36].

Table 2. Average value of index change by category

Index	Non-Abrasion (0)	Abrasion (1)
ΔMVI	0.206443	-0.28326
ΔTCI	-0.319361	0.438194
ΔNDVI	0.420855	-0.577454
ΔLSWI	-0.000786	0.001078

3.2. Classification of Abrasion Areas

Data extracted from satellite photos will be utilized to predict the classification of abrasion zones through machine learning techniques. The modeling step encompasses multicollinearity assessment, machine learning model creation, evaluation of model performance, essential feature selection, and classification analysis of abrasion-susceptible regions on Panaitan Island.

3.2.1. Multicollinearity Test

This investigation necessitates a multicollinearity test due to the utilization of logistic regression. The test findings demonstrate that all VIF values for the variables in this study are below 10 (VIF <10).

The VIF test findings indicate no multicollinearity in the data. By adhering to the criteria for multicollinearity, all independent variables may be utilized in the training and validation processes to identify optimal parameters and evaluate estimations.

3.2.2. Classification Models

This study analyzes machine learning algorithms based on supervised learning, specifically Random Forest, Support Vector Machine, and Logistic Regression. The optimal parameter search was conducted via Bayesian optimization with k-fold cross-validation [37]. The findings indicate that the ideal parameters for Random Forest are a max_depth of 8, max_features of 0.9395, min_samples_leaf of 4, min_samples_split of 7, n_estimators of 42, and random_state of 42. The ideal settings for the Support Vector Machine are C = 10, gamma = 1, and a linear kernel. Logistic Regression attains optimal performance with C = 0.1, max_iter = 100, solver = liblinear, and a balanced class weight.

3.2.3. Machine Learning Model Performance

Model evaluation is an essential process for identifying the optimal model. The evaluation of the classification model in this study was performed utilizing accuracy, precision, recall, and F1-score [34]. The subsequent evaluation measures pertain to each machine learning algorithm. The subsequent evaluation measures pertain to each machine learning algorithm. However, the analysis is limited to the period between 2018 and 2023, The spatial resolution of the data, derived from Landsat 8 and Sentinel-2 at 20 × 20 m per record in coastline area Panaitan's island, generates a large dataset that is effectively suitable for machine learning applications.

According to Table 3, the Random Forest model demonstrated superior performance compared to the other machine learning algorithms evaluated in this study. This model achieved an accuracy of 82.23%, with a precision of 0.82, a recall of 0.82, and an F1-score of 0.82, indicating a balanced and robust classification capability for both abrasion and non-abrasion classes. The strong performance of Random Forest can be attributed to its ability to handle nonlinear relationships and complex interactions among environmental variables without requiring strict distributional assumptions. Moreover, Random Forest is less sensitive to noise and multicollinearity than parametric models, making it particularly suitable for large, high-dimensional datasets derived from multi-source satellite imagery. Consequently, this model was selected to further analyze feature importance and assess the relative contribution of each environmental variable to shoreline abrasion classification.

Table 3. Machine learning model performance

Parameter	Random forest	Support vector machine	Logistic regression
Accuracy	0.8223	0.7434	0.7422
Precision	0.82	0.76	0.75
Recall	0.82	0.74	0.74
F1-score	0.82	0.74	0.74

3.2.4. Feature Importance

Feature importance for identifying factors that significantly influence the constructed model, as illustrated in Figure 7. NDVI is the most significant variable in the model. The values of each variable in the abrasion categorization are as follows: NDVI is 0.5304, TCI is 0.2131, LSWI is 0.154, and MVI is 0.1025. While NDVI exerts the most significant influence, all variables contribute quite uniformly to the model. This contrasts with another research, who determined that NDVI exerts only a 6.5% influence on coastline alterations, which is statistically insignificant [16]. This research in line with other researches indicating that vegetation mitigates wave action, preserves soil moisture, endures wind, and stabilizes sediment [7, 38, 39]. Climate change has widespread impacts on maritime and coastal sectors, leading to rising temperatures, sea-level rise, and extreme weather events, which contribute to coastal abrasion that threatens ecosystems and coastal communities [1].

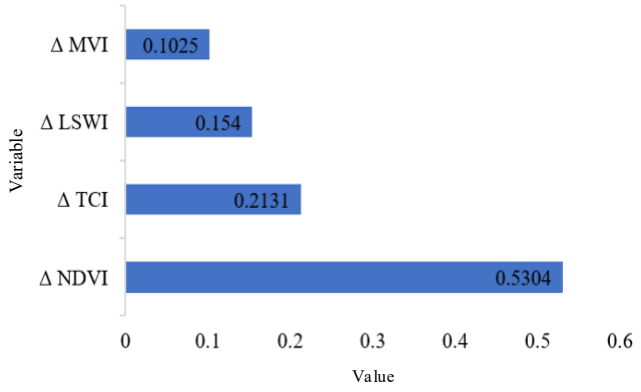

Figure 7. Feature importance graph random forest model

3.3. Area Estimation and Classification Analysis of the Abrasion Area of Panaitan Island

Spatial analysis conducted using QGIS indicates that Panaitan Island experienced shoreline abrasion covering an estimated area of 2.04 km² during the period 2018–2023, out of a total land area of 125.77 km² in 2023. Areas affected by abrasion are generally characterized by noticeable reductions in the density of green vegetation, particularly coastal forests and mangroves that play a critical role in stabilizing shorelines and dissipating wave energy. Correlation analysis shows that changes in soil conditions and moisture, as represented by LSWI, do not exhibit a strong linear relationship with abrasion occurrence. However, the machine learning results demonstrate that these variables still contribute meaningfully to abrasion classification, suggesting that their influence may be nonlinear or interact with other environmental factors. This finding underscores that shoreline abrasion on Panaitan Island is driven by a combination of vegetation degradation and environmental dynamics rather than by a single dominant factor.

4. Conclusion

This study employs remote sensing data from Panaitan Island, Banten, comprising 11,545 coastal records, to classify abrasion-prone areas based on variations in vegetation density (NDVI), mangrove density (MVI), soil moisture (LSWI), and surface temperature (TCI) using machine learning, identifying Random Forest as the best-performing model (82.23% accuracy) with NDVI as the most influential factor, estimating approximately 2.04 km² of abraded area from 2018 to 2023 linked to human activities such as illegal road construction and logging, while surface temperature, climatic changes, and vegetation conditions also serve as key indicators. The classification could achieve better performance if additional marine environmental variables, such as wave height and length, were included, although the study remains limited by its temporal span, spatial resolution, and unobserved environmental factors.

Ethics approval

Not required.

Acknowledgments

The author wishes to convey appreciation to the Ujung Kulon National Park Unit for its website and pertinent information concerning the natural conditions of Panaitan Island. The author extends profound gratitude to Mr. Robert for his helpful feedback and ongoing support during the study's development.

Competing interests

All the authors declare that there are no conflicts of interest.

Funding

This study received no external funding.

Underlying data

This research uses secondary data from the Google Earth Engine (GEE) Data Catalog.

Credit Authorship

Ghaffar Ismail: Conceptualization, Methodology, Writing, Editing, Visualization. **Robert Kurniawan:** Reviewing, Methodology, Validation, Editing, Supervision. **Silvia Ni'matul Maula:** Data Curation, Editing, Validation.

References

[1] N. S. Gravitiani, E., Rahardjo, M., & Pratiwi, "Apakah turis bersedia membayar untuk mitigasi abrasi? Sebuah studi di daerah pesisir di Yogyakarta, Indonesia," *Glob. J. Bus. Soc. Sci. Rev.*, pp. 5(2), 46–51, 2017, [Online]. Available: https://ssrn.com/abstract=3002423

[2] D. Paprotny, P. Terefenko, A. Giza, P. Czapliński, and M. I. Vousdoukas, "Future losses of ecosystem services due to coastal erosion in Europe," *Sci. Total Environ.*, vol. 760, p. 144310, 2021, doi: 10.1016/j.scitotenv.2020.144310.

[3] F. Cai, X. Su, J. Liu, B. Li, and G. Lei, "Coastal erosion in China under the condition of global climate change and measures for its prevention," *Prog. Nat. Sci.*, vol. 19, no. 4, pp. 415–426, 2009, doi: 10.1016/j.pnsc.2008.05.034.

[4] M. A. Marfai, *Catatan kecil tentang informasi geospasial (Edisi ke-1)*. Badan Informasi Geospasial, 2023.

[5] Y. Deslatama, "Tidak dirawat, 2 pulau di Banten hilang," Liputan6.com. Accessed: Feb. 20, 2025. [Online]. Available: https://www.liputan6.com/news/read/2253209/tidak-dirawat-2-pulau-di-banten-hilang

[6] Balai Taman Nasional Ujung Kulon, "Taman Nasional Ujung Kulon," Kementerian Lingkungan Hidup dan Kehutanan Republik Indonesia. Accessed: Mar. 28, 2025. [Online]. Available: https://tnujungkulon.menlhk.go.id/

[7] A. Hakam, B. Istijono, and T. Ophiyandri, "Vegetations as beach protection: Simulations of root protection mechanism against abrasion," *Int. J. Adv. Sci. Eng. Inf. Technol.*, vol. 7, no. 6, pp. 2316–2321, 2017, doi: 10.18517/ijaseit.7.6.3445.

[8] Dinas Lingkungan Hidup dan Kehutanan Prov. Banten, "Updating data luas kawasan mangrove di Provinsi Banten," 2023.

[9] G. Kaplan and U. Avdan, "Mapping and monitoring wetlands using sentinel-2 satellite imagery," *ISPRS Ann. Photogramm. Remote Sens. Spat. Inf. Sci.*, vol. 4, no. 4W4, pp. 271–277, 2017, doi: 10.5194/isprs-annals-IV-4-W4-271-2017.

[10] R. Bishop-Taylor, R. Nanson, S. Sagar, and L. Lymburner, "Mapping Australia's dynamic coastline at mean sea level using three decades of Landsat imagery," *Remote Sens. Environ.*, vol. 267, no. March, p. 112734, 2021, doi: 10.1016/j.rse.2021.112734.

[11] M. N. Nandaniko, Supriatna, and M. D. M. Manessa, "Modeling of coastline change by viewing trends from the abrasion and accretion rate in karawang regency," *IEEE*, pp. 0–4, 2019, doi: 10.1109/ICST47872.2019.9166274.

[12] A. B. Baloloy, A. C. Blanco, R. R. C. Raymund Rhommel, and K. Nadaoka, "Development and application of a new mangrove vegetation index (MVI) for rapid and accurate mangrove mapping," *ISPRS J. Photogramm. Remote Sens.*, vol. 166, no. January, pp. 95–117, 2020, doi:

10.1016/j.isprsjprs.2020.06.001.
[13] F. N. Kogan, "Global drought watch from space," *Bull. Am. Meteorol. Soc.*, vol. 78, no. 4, pp. 621–636, 1997, doi: 10.1175/1520-0477(1997)078<0621:GDWFS>2.0.CO;2.
[14] Y. Zhou *et al.*, "Open surface water mapping algorithms: A comparison of water-related spectral indices and sensors," *Water (Switzerland)*, vol. 9, no. 4, 2017, doi: 10.3390/w9040256.
[15] A. Ghorbanian, S. Zaghian, R. M. Asiyabi, M. Amani, A. Mohammadzadeh, and S. Jamali, "Mangrove ecosystem mapping using sentinel-1 and sentinel-2 satellite images and random forest algorithm in google earth engine," *Remote Sens.*, vol. 13, no. 13, pp. 1–18, 2021, doi: 10.3390/rs13132565.
[16] E. D. Kusumaningrum, A. Saputra, and A. Nurwijayanti, "Analysis of vegetation density changes on coastline changes in the Glagah Coastal Area, Kulon Progo Regency 2018 and 2023," *IOP Conf. Ser. Earth Environ. Sci.*, vol. 1357, no. 1, 2024, doi: 10.1088/1755-1315/1357/1/012009.
[17] A. Rahman *et al.*, "Remote sensing applications: Society and environment performance of different machine learning algorithms on satellite image classification in rural and urban setup," *Remote Sens. Appl. Soc. Environ.*, vol. 20, no. July, p. 100410, 2020, doi: 10.1016/j.rsase.2020.100410.
[18] M. Mahapatra, R. Ratheesh, and A. S. Rajawat, "Shoreline change analysis along the coast of South Gujarat, India, using digital shoreline analysis system," *J. Indian Soc. Remote Sens.*, vol. 42, no. 4, pp. 869–876, 2014, doi: 10.1007/s12524-013-0334-8.
[19] D. N. D. Pratama, N. Khakhim, A. Wicaksono, A. Musthofa, and W. Lazuardi, "Spatio-temporal analysis of abrasion susceptibility effect on land cover in the coastal area of Bantul regency, Yogyakarta, Indonesia," *Int. J. Geoinformatics*, vol. 17, no. 4, pp. 109–126, 2021, doi: 10.52939/ijg.v17i4.1961.
[20] B. Deepika, K. Avinash, and K. S. Jayappa, "Shoreline change rate estimation and its forecast: Remote sensing, geographical information system and statistics-based approach," *Int. J. Environ. Sci. Technol.*, vol. 11, no. 2, pp. 395–416, 2014, doi: 10.1007/s13762-013-0196-1.
[21] T. M. Berhane *et al.*, "Decision-tree, rule-based, and random forest classification of high-resolution multispectral imagery for wetland mapping and inventory," *Remote Sens.*, vol. 10, no. 4, 2018, doi: 10.3390/rs10040580.
[22] I. N. Hidayati, R. Suharyadi, and P. Danoedoro, "Kombinasi indeks citra untuk analisis lahan terbangun dan vegetasi perkotaan," *Majalah Geografi Indonesia*, vol. 32, no. 1, p. 24, 2018. [Online]. Available: https://doi.org/10.22146/mgi.31899
[23] R. H. J. Bagus Pamungkas, "Pemanfaatan citra pengindraan jarak jauh dan sistem informasi geografis untuk pemetaan erosi di DAS Serang Kabupaten Kulon Progo," *Jurnal Bumi Indonesia*, vol. 15, no. 1, pp. 165–175, 2016.
[24] M. Conopio, A. B. Baloloy, J. Medina, and A. C. Blanco, "Spatio-Temporal mapping and analysis of mangrove extents around manila bay using landsat satellite imagery and mangrove vegetation index (MVI)," *Int. Arch. Photogramm. Remote Sens. Spat. Inf. Sci. - ISPRS Arch.*, vol. 46, no. 4/W6-2021, pp. 103–108, 2021, doi: 10.5194/isprs-Archives-XLVI-4-W6-2021-103-2021.
[25] M. P. Neri, A. B. Baloloy, and A. C. Blanco, "Limitation assessment and workflow refinement of the mangrove vegetation index (mvi)-based mapping methodology using sentinel-2 imagery," *Int. Arch. Photogramm. Remote Sens. Spat. Inf. Sci. - ISPRS Arch.*, vol. 46, no. 4/W6-2021, pp. 235–242, 2021, doi: 10.5194/isprs-Archives-XLVI-4-W6-2021-235-2021.
[26] S. Huang, L. Tang, J. P. Hupy, Y. Wang, and G. Shao, "A commentary review on the use of normalized difference vegetation index (NDVI) in the era of popular remote sensing," *J. For. Res.*, vol. 32, no. 1, pp. 1–6, 2021, doi: 10.1007/s11676-020-01155-1.
[27] X. Zhao, H. Xia, L. Pan, H. Song, W. Niu, R. Wang, R. Li, X. Bian, Y. Guo, and Y. Qin, "Drought monitoring over yellow river basin from 2003–2019 using reconstructed MODIS land surface temperature in google earth engine," *Remote Sens.*, vol. 13, no. 18, 2021, doi: 10.3390/rs13183748.
[28] J. Brema, T. S. Rahul, and J. J. Julius, *Study on Drought Monitoring Based on Spectral Indices in Noyyal River Sub-watershed Using Landsat-8 Imageries*. Springer International Publishing, 2019. doi: 10.1007/978-3-319-77276-9_42.
[29] M. W. Browne, "Cross-validation methods. Journal of Mathematical Psychology," *J. Math. Psychol.*, vol. 44, pp. 108–132, 2000.
[30] N. Shrestha, "Detecting multicollinearity in regression analysis," *Am. J. Appl. Math. Stat.*, vol. 8, no. 2, pp. 39–42, 2020, doi: 10.12691/ajams-8-2-1.

[31] L. Breiman, "Support vector machines for classification and regression. Analytical Methods," *Int. J. Adv. Comput. Sci. Appl.*, vol. 7, no. 6, pp. 135(2), 230–240, 2001, doi: 10.1039/b918972f.
[32] A. Fernández, S. García, F. Herrera, and N. V. Chawla, "SMOTE for learning from imbalanced data: Progress and challenges, marking the 15-year anniversary," *J. Artif. Intell. Res.*, vol. 61, pp. 863–905, 2018, doi: 10.1613/jair.1.11192.
[33] J. R. Wilson and K. A. Lorenz, "Short history of the logistic regression model," pp. 17–23, 2015, doi: 10.1007/978-3-319-23805-0_2.
[34] W. P. Chawla, N. V., Bowyer, K. W., Hall, L. O., & Kegelmeyer, "SMOTE: Synthetic minority over-sampling technique," *J. Artif. Intell. Res.*, pp. 16, 321–357, 2002, doi: 10.1613/jair.953.
[35] K. Ichii, A. Kawabata, and Y. Yamaguchi, "Global correlation analysis for NDVI and climatic variables and NDVI trends: 1982–1990," International Journal of Remote Sensing, vol. 23, no.
[36] Z. Feng, X. Wang, J. Yuan, Y. Zhang, and M. Yu, "Changes in air pollution, land surface temperature, and urban heat islands during the COVID-19 lockdown in three Chinese urban agglomerations," Science of the Total Environment, vol. 892, art. no. 164496, 2023.
[37] P. I. Frazier, "A tutorial on bayesian optimization," CoRR, vol. abs/1807.02811, Jul. 2018.18, pp. 3873–3878, 2002.
[38] M. A. Wojtas and K. Chen, "Feature importance ranking for deep learning," *Adv. Neural Inf. Process. Syst.*, vol. 2020-Decem, no. NeurIPS, 2020.
[39] D. C. Donato, J. B. Kauffman, D. Murdiyarso, S. Kurnianto, M. Stidham, and M. Kanninen, "Mangroves among the most carbon-rich forests in the tropics," *Nat. Geosci.*, vol. 4, no. 5, pp. 293–297, 2011, doi: 10.1038/ngeo1123.